Understanding the stability and structural properties of ordered nanoporous metals towards their rational synthesis

Authors for correspondence:
C. Richard A. Catlow
e-mail: c.r.a.catlow@ucl.ac.uk
A. Rabdel Ruiz-Salvador
e-mail: rruisal@upo.es
Said Hamad
e-mail: said@upo.es

†These authors equally contributed to this study.

Jose M. Ortiz-Roldan[1,†], Salvador R. G. Balestra[1,2,†], Rocio Bueno-Perez[3], Sofía Calero[1,4], Elena Garcia-Perez[1], C. Richard A. Catlow[5,6,7], A. Rabdel Ruiz-Salvador[1] and Said Hamad[1]

[1]Department of Physical, Chemical and Natural Systems, University Pablo de Olavide, Ctra. Utrera km. 1, 41013, Seville, Spain
[2]Consejo Superior de Investigaciones Científicas, Instituto de Ciencia de Materiales de Madrid, c/ Sor Juana Inés de la Cruz, 3, 28049 Madrid, Spain
[3]Adsorption & Advanced Materials Laboratory (A2ML), Department of Chemical Engineering & Biotechnology, University of Cambridge, Philippa Fawcett Drive, Cambridge CB3 0AS, UK
[4]Materials Simulation and Modeling, Department of Applied Physics, Eindhoven University of Technology, Netherlands
[5]Department of Chemistry, University College London, 20 Gordon St., London WC1H 0AJ, UK
[6]UK Catalysis Hub, Research Complex at Harwell, STFC Rutherford Appleton Laboratory, Chilton, Oxon OX11 0FA, UK
[7]School of Chemistry, Cardiff University, Cardiff CF10 1AT, UK

SRGB, 0000-0002-2163-2782; RB-P, 0000-0002-1472-6852; SC, 0000-0001-9535-057X; CRAC, 0000-0002-1341-1541; ARR-S, 0000-0002-2004-687X; SH, 0000-0003-4148-2344

Ordered Nanoporous Metals (ONMs) form a new family of nanoporous materials composed only of pure metals. The expected impact is considerable from combining the ordered nanopore structure of MOFs, zeolites and carbon schwartzites with the robustness and electronic conductivity of metals. Little is known about their stability and structural features.

Here we address these points to provide clues toward their rational synthesis, introducing an automatic atomistic design that uses model building and molecular dynamics structural relaxation, and is validated against the experimentally known ONMs. Analysing the properties of the 10 stable structures out of the 17 studied (14 of which are designed in this work) using four noble metals (Pt, Pd, Au and Ag), we have deciphered some key elements and structural descriptors that provide guidelines for the experimental synthesis of ONMS. The long-lived metastability of the stable ONMs is evidenced by the high free energy landscape, computed via Metadynamic simulations. The new ONMs permit molecular diffusion of various molecules of industrial relevance, increasing the expectation for their use in catalysis, separation, nanofiltration, batteries, fuel cells, etc. Stable low-cost ONMs are predicted using Earth-abundant Ni metal, which maintains the main features of their relative noble metal forms.

1. . Introduction

Nanoporous materials, such as zeolites, Metal-Organic Frameworks (MOFs) and Covalent-Organic Frameworks (COFs), characterized by large surface-to-volume ratios, play a major role in a plethora of chemical technologies, owing to their good catalytic, ion-exchange, adsorption and separation properties [1,2]. A new family of nanoporous solids, called Ordered Nanoporous Metals (ONMs), was recently synthesized [3], with the special feature of being composed only by metal atoms. ONMs have porosities similar to those of traditional porous solids, but they also share the robustness, electronic and catalytic properties of metals. The strategy used for synthesizing these first ONMs resembles that followed in the preparation of zeolite-replicated carbon (ZRC) materials [4]. The method devised for casting these ONMs structures consisted of introducing K_2PtCl_4 molecules into the pores of the templating MOFs. These molecules are subsequently reduced and the templating MOF is etched with hydrofluoric acid. As expected, the resulting new metal nanostructures exhibit excellent catalytic activity in methanol electrooxidation reactions. A more recent work reports that a mesoporous trimetallic PtPdAu alloy exhibits enhanced electrocatalytic activity in methanol oxidation [5].

Porous metals can be prepared by diverse routes, dealloying being the most common, with an increasing number of methods that provide more flexibility in the synthesis, such as templating, combustion synthesis and colloidal chemistry, which allow the assembly of nanoparticles, nanotubes or nanorods to create various porous structures, including nanofoams [6–11]. In these materials, the high electronic conductivity is coupled with a high surface area, associated with the porosity, to produce high-performance electrodes for batteries, fuel cells and supercapacitors [6,8]. The high surface area of these metallic nanostructured materials also allows their use in sensing, by exploiting surface-enhanced Raman scattering (SERS) as well as in catalysis, either as an active phase, simple support, or a combination of both [7,8,10,11]. There are two main differences between ONMs and disordered, dealloyed nanoporous metals. By contrast to traditional porous metals, in which usually there are no connected molecular-scale voids throughout the material, the ordered nature of the porosity in ONMs guarantees the existence of this sort of connected free nanospaces, allowing controlled mass transport in the whole volume, and also providing a narrow pore size distribution (a key aspect in size-selectivity). Moreover, the ordered templating hosts not only translate to the nanocasted ONMs their ordered negative replica topology, but also their pore regularity. This is an important property for shape-regulated applications, such as adsorption, separation and catalysis. This property permits the fine tuning of the performance of ONMs as advanced electrodes in traditional areas of electrochemistry where porous metals can be used, like batteries, fuel cells and supercapacitors. From the knowledge in the field of ZRC materials, where hundreds of hypothetical nanoporous solids have been designed (and in some cases later synthesized) from known zeolites [12,13], we can expect that the large numbers of known MOFs would stimulate the conceptual design of a very large set of potential ONMs. Moreover, the wide horizon of synthesizable materials provides unprecedented flexibility to the

design of potential topologies of ONMs, which will allow a rational selection of the best material for targeted applications, in terms of pore sizes and selectivity. By achieving such developments, one would expect a significant step forward in the state of the art in porous metals. Such developments are in an embryonic stage, and systematic studies on the stability and structural properties of ONMs are still needed.

In this pioneering predictive work, we aim to fill some primary gaps concerning the design of stable ONMs, and the understanding of their stability and structural properties, as well as to provide guidelines for their rational synthesis. In their initial work, Gao *et al.* [3] simulated the structure of three ONMs, assuming a continuous occupation of the MOF channels by the metal. Their predicted diffraction patterns were in good agreement with the experimental ones. This approach was based on filling the pores with a continuous metal body. From an atomistic design point of view, it is worth noting that such an approach cannot be applied to the related analogues, zeolite-replicated carbon materials, since the directional C–C bonds appearing in carbons impose severe structural constraints. In 2007, seven years after the experimental discovery of ZRCs, Rousel *et al.* [14] used Monte Carlo simulations to absorb carbon atoms that fill the pores and generate ZRCs frameworks [14,15]. They showed the utility of the approach used for *in silico* building of ZRCs models, although the density of the solids was higher than experiment. Two years later, Nishihara *et al.* showed that a Lego-like construction of atomistic models using hexagons, pentagons and/or heptagons assembled to graphene sheets can be used to simulate the structure of ZRCs [16]. Further developments in both approaches have appeared in recent years [12,17].

We note that the widely used codes that employ the traditional Monte Carlo method (based on sampling of possible displacements and atom insertion/deletion) are expected to show poor performance in designing ONMs, in terms of the ratio quality/computer time. While those codes are a useful tool to create ZRCs, our preliminary simulations on OMNs showed that the number of atoms (in the order of tens of thousands versus only hundreds or few thousands in ZRCs) exceeds the practical limits for efficient Monte Carlo full loading simulations of porous materials.

To be able to predict new ONMs with tailored structures and chemical compositions for targeted applications, we would need first to answer the hitherto untreated questions about the stability of this family of materials. Among others, the following key questions are still open. Is there a relation between the stability of these solids and their densities? Which metals can be used to form OMNs and why? What is the relative energy of these ONMs with respect to the most stable solid built with the same metal? Is there a local structural descriptor for predicting the suitability of the synthesis? In this way, our goal here is to obtain new knowledge about the general features of the family of ONMs, for which we use two noble metals, Pt and Pd, already employed for the preparation of monometal ONMs [3], Au, which has been used in a trimetallic ONM [5] and Ag, which has not been used yet. A secondary motivation for studying the stability and structural features of ONMs of different chemical compositions is to gain an understanding so as to predict ONMs built by metal atoms whose cost would be much smaller than those of the noble metals Pt, Pd and Rh. Their high cost represents a practical handicap for the large-scale use of ONMs.

Here we introduce a simple computational approach to carry out the *in silico* design of stable ONMs, which we validate by reproducing the stability of the experimentally prepared ONMs by Gao *et al.* [3]. Besides MOFs, we also use large pore supertetrahedral (ST) solids [18] as hard-templating solids. The exploration of the stability of the *in silico*-built ONMs has been conducted by combining the analysis of structural, energetic and dynamical features extracted from large-scale molecular dynamics simulations with the analysis of the free energy profiles for atomic diffusion on an internal pore surface, calculated by Metadynamic simulations. We should note that the thermodynamically stable metal structures are non-porous and that when we refer to an ONM as stable we are indicating that it has a long-lived metastable porous structure, as shown by our simulations or, in some cases, by experiment. This is analogous to the case of porous silicate structures, which are less stable than the corresponding dense structures, but which can remain porous, such as zeolitic minerals, for millions of years [19]. Since transport properties of guest

molecules are relevant properties needed for catalysis, adsorption and separation applications, as well as for more efficient performance in electrochemical areas, we compute the diffusion coefficients of the ortho, meta and para isomers of xylene, water, benzene and methanol. The choice of these molecules lies in their relevance in the green production of fuels and other chemical feedstocks.

2. Computational methods

(a) Construction of the models

Our atomistic computational design of ONMs combines a geometric approach, to build the initial structures, with structural relaxation. The nature of the bonds in metals, which are not directionally restrictive, permits the use of a geometrical approach for generating the starting atomistic models. Our method proceeds through the following steps: (1) we create a supercell of the metal atoms in the bulk, crystalline phase, with FCC symmetry, in such a way that the cell parameters are as close as possible to those of the hard-templating solid; (2) the atoms of the original templating structure are also inserted into the cell, (3) all the overlapping metal atoms (i.e. all metal atoms at a distance less than the sum of van der Waals radii from any framework atom) are removed; (4) we identify those metal atoms with numbers of connections to other metal atoms below three, and remove them, leaving the ONMs with the allowed connectivity for all metal atoms and (5) we perform a structural relaxation, in two steps: first a smooth relaxation at 0 K, and then a simulation at higher temperatures using MD. Doing this, we can account for the deviations from the initial structure that are expected to occur, such as reconstructions of the internal surfaces to achieve more favourable pore morphologies. The results allow us to evaluate the stability of the materials. The structural relaxation can be relevant near the internal surface of the solids, where the bulk-like atom connectivity assumed in the initial geometrical construction can be modified. This is in line with the High Resolution Transmission Electron Microscopy (HRTEM) results on ONMs samples obtained by Gao *et al.,* which show bulk-like atomic sections [3]. One secondary, but relevant, consequence of the connectivity of the metal atoms is that electronic conductivity is expected to remain high, although it might decrease with respect to that of bulk metals, retaining the metallic conductivity, as occurs in metal nanowire networks [20] and ZRCs [21].

(b) Atomistic simulation methods of the structure and related properties

The initial construction of the solids resulted in periodic units containing several thousand atoms, which precludes the use of Density Functional Theory (DFT) calculations. Therefore, the structural and dynamical properties of the solids were studied by classical molecular dynamics (MD) simulations with the LAMMPS code [22], using long-range Embedded Atom Method (EAM) interatomic potentials. To ensure larger transferability of the potentials, as compared with those obtained from fitting experimental data at bulk crystallography conditions, we selected first-principles derived interatomic potentials by Sheng *et al.* [23]. To allow a flexible parameterization, the authors built a large set of configurations that include crystal structures, defects, the fcc-bcc Bain deformation path and the trigonal Bain deformation path and liquid structures. Moreover, they used a large cut-off to act as a surrogate for the lack of angular description. Note that this is particularly useful in modelling complex atomic environments, where a variety of local structures can appear and thus the use of angular terms is expected to artificially bias the structure toward predetermined atomic environments. We must note that these potentials are not only applicable to bulk systems, but they have also proved to be useful to model different nanosystems [24–27]. Details of the potentials [23,24] employed are reported in the supplementary information.

A preliminary set of calculations indicated that some ONMs collapsed after 500 ps of MD simulations, which suggested that long MD runs are required to ensure the assessment of stability of these materials. Stable structures should exhibit stationary behaviour of the potential energy

and cell parameters, once the simulations are equilibrated. In electronic supplementary material, figure S1, these magnitudes are plotted for the Pt-CRI-ST3 ONM (see below) at 300 K, as an example. The slopes values close to zero are indicative of the stationary behaviour. We must note that the energy fluctuations over the whole simulation time are lower that the thermal fluctuation energy (kT). The variation of the cell parameter is within the error bar of the determinations from room temperature powder diffraction patterns. Thus, we numerically checked their stationary behaviour, and since this is a key point in the design of a new class of materials, we conducted 100 ns long MD simulations. In a realistic and challenging test, the simulations have been carried out in the isothermal-isobaric (NPT) ensemble, in order to test the stability with respect to structural collapse. The preliminary simulations indicated that the artificial constraint imposed in canonical MD simulations, associated with the use of fixed cell parameters, precludes the use of such simulations to gauge the stability since unstable structures erroneously appear as stable. Using Ni-CRI-ST3 as an example, we observe that the material would appear to be stable at 1000 K in NVT MD simulations (electronic supplementary material, figure S2), whereas it will be shown below that this ONM collapses at temperatures above 900 K when modelled with the more realistic NPT MD simulations. As a result of significant diffusion of the internal surface metal atoms, non-porous structures are formed after the collapse of the ONMs at certain temperatures, i.e. the materials either kept the nanoporosity or they become totally non-porous. The two indicators mentioned above, cell parameters and potential energy, allow the identification of local collapse before a subsequent total collapse occurs. The Nosé-Hoover thermostat and barostat were used, with time constants of 0.1 and 2 ps, respectively. A time step of 1 fs was employed for the calculations, and 500 ps were used for the equilibration. Since atomic rearrangements are expected to occur, due to the structural evolution after the initial *in silico* construction, we tried to avoid large atomic single-step motions, to ensure smooth stress relaxation without artificial collapse. For this reason, the time step was chosen to be 1 fs, shorter than the time step that could be used when simulating the bulk metal. Previous to the design of new ONMs, the described methodology is first validated by reproducing the structure and stability of three experimentally reported ONMs [3].

Having stationary behaviour of the cell parameters and potential energy is necessary, but not sufficient to guarantee stability from a macroscopic point of view, where the materials should last at least hours. But even this relatively small timescale is inaccessible in MD simulations. It would be desirable to show that the materials remain in this stationary behaviour for a long time. By analysing the trajectories of the previous unbiased MD simulations, we discovered that in the moments before the structural collapse of the unstable ONMs, some low-coordinated atoms started to slide along the inner surface of the pore, accumulating in certain regions, which generates a distortion that disrupts the internal equilibrium of the ONM and triggers the collapse to the dense phase. So, by performing Metadynamics (MetaD) simulations with Adaptive Gaussians [28,29] we sampled these events in an efficient way to determine the energy barriers of the primary steps toward local disordering of the materials, by exploiting the capabilities of the LAMMPS, coupled with the code PLUMED [30–32]. The attention was focused on the evolution of atoms in relevant distinct environments on the pore internal surface, namely a mostly planar-like environment and highly curved (corner-like) environments. The centre of mass of each atomic environment was selected as reference point, and the distance from the diffusing atom to the reference point was used as a collective variable in the MetaD analysis, with which to calculate the free energy barriers for the diffusion of surface atoms. The Well-Tempered MetaD simulations were performed with the multiple walker enhanced sampling technique, using four walkers that were run with eight cores each. More information about the MetaD simulations, PLUMED inputs and the environment definitions can be found in electronic supplementary material, figure S3 and Plumed input Code S1 in the electronic electronic supplementary material, (ESI).

Since one of the primary goals of using metal nanostructured solids is to exploit their potential thermo-structural stability for applications at temperatures well above room temperature, some thermal properties were studied, such as the specific heat at constant pressure (C_P) and the thermal expansion for the temperature range where each ONM is stable. The thermal expansion

was studied by means of a series of MD simulations at increasing temperatures, where the temperature was varied slowly enough to permit the system to reach equilibrium at every temperature. We increased the temperature at a rate of $0.1 \, \mathrm{K \, ps^{-1}}$. The thermal expansion coefficient, α, and the specific heat, C_P, were calculated with the standard procedures, which use the calculated variation of the lattice parameter or the total energy with respect to temperature (see details in the electronic supplementary material).

(c) Molecular transport

Here, we do not focus on the detailed study of the molecular diffusion in these materials; our goal is to know whether they permit diffusion through their pores. The diffusion coefficients of the molecules investigated in the generated ONMs structures were calculated by fitting the Mean Squared-Displacement (MSD) in the production period of the MD simulations at 300 K (see electronic supplementary material, figure S5). Molecular loadings half of their maximum adsorption capacity were employed, for each molecule. The maximum adsorption capacity for each molecule was estimated from the bulk density of the adsorbate and the void volume fraction inside the metal pore. The MD simulations were carried out in the NPT ensemble, considering long enough simulation times (ranging from 10 to 20 ns) to ensure that the MSD exceeds the lattice parameter of the cell. In these simulations all atoms were allowed to move. Water molecules were modelled using the TIP3P force field [33]. Methanol, the three xylene isomers and benzene molecules were modelled with DREIDING force field [34]. The intermolecular interactions between the metal atoms and the adsorbed molecules were accounted for with the well-tested, non-generic force fields by Jalkanen *et al.* [35], and Tarmyshov *et al.* [36], and Heinz *et al.* [37], for silver, platinum and nickel ONMs, respectively. The development of accurate force fields with which to model host–guest interactions specifically for ONMs would require an arduous job of fitting the parameters, using high-level electron structure calculations capable of a chemical-accuracy consideration of weak intermolecular interactions, so we have used existing force fields. For this reason, the results we obtain must be regarded as qualitative information about how diffusion would take place in these materials, not as accurate, quantitative information. To facilitate the reproducibility of the results and to allow further developments, in the supplementary material, we provide as examples the files used for modelling the system xylene-Ag-CRI-ST3-ONM.

The porosity and textural properties were computed with RASPA code [38], for OMNs, and with Poreblazer [39], for MOFs and ST solids. Besides surface area and pore volume, for all solids, the pore size distribution was used to determine the largest pore aperture in OMNs, while the large cavity diameter (LCD) and pore limiting diameters (PLD) were also determined for MOFs and ST solids.

3. Results and discussion

(a) Conceptual design and atomistic model building

A schematic view of the construction of the ONMs designed in this study is illustrated in figure 1. In order to show the relation between the ONM and the original sacrificial hard template framework, in the left side, we include a shaded view of the supertetrahedral (ST) solid with SOD zeolite topology used in this case, while its designed negative replica ONM is shown on the right, which is the structure left once the original template is etched.

In the atomistic design of ONMs, we would need to consider in first place the non-directional nature of the chemical bond in metals, as opposed to zeolites, MOFs and carbon schwartzites, where directional bonds stabilize low-symmetry local atomic environments. The lack of such bonds in metals might induce atomic surface diffusion, with relatively low activation energy. Consequently, the large internal surface of a metallic nanoporous solid would be at risk of structural damage, resulting from the migration of labile atoms, mainly those acting as
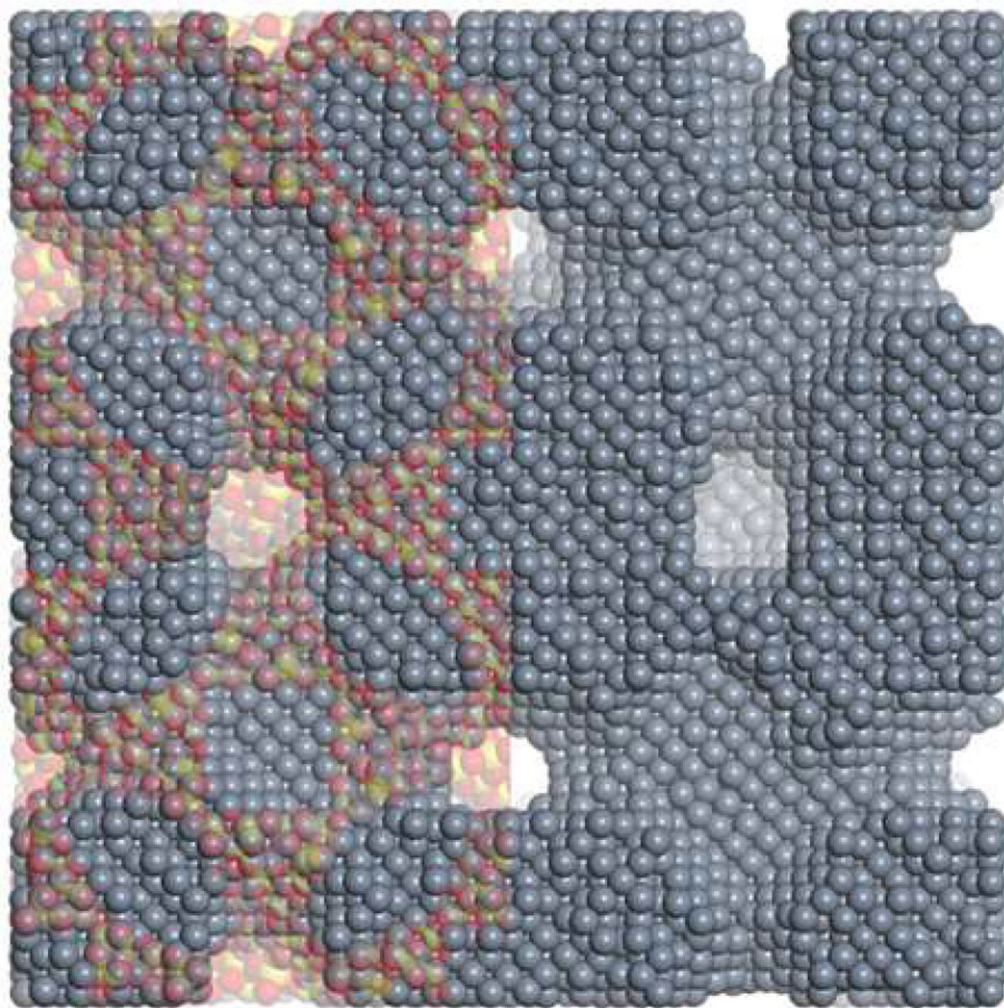
Figure 1. Shaded view of the supertetrahedral solid (left) with SOD zeolite topology, which is filled with metal atoms to form the initially unrelaxed ONM (right). The ONM is obtained once the original sacrificial hard template framework is removed. (Online version in colour.)

connectors, and therefore leading to framework collapse. For this reason, we propose to design nanoporous solids with pore walls several atomic layers wide, so that large-pore templating solids are needed, such as MOFs or ST solids for instance. This structural requirement induces a clear difference between ONMs and ZRCs, where a wall of a single atom width can be stable, allowing the use of zeolites as templates, which have smaller pores than those that can exhibit some MOFs and ST solids. Another essential structural feature that the templating materials should exhibit is the presence of three-dimensional pore connectivity, in order to ensure a three-dimensional solid as its negative replica. If the templating material only had pore connectivity in one or two directions, the metal nanostructures thus generated would consist of a series of one-dimensional metal nanorods or a series of two-dimensional metal nanolayers.

In order to validate the approach to generate stable *in silico* ONMs, we first apply the procedure to the three ONM structures experimentally reported by Gao *et al.* [3] (see supporting information to see the structures). We used Pt as the constituent metal, to be compliant with the experiment, and found that the structures remain stable at room temperature for the ONM built from MOF-808, PCN-777 and BUT-12. The structural collapse appears at *ca* 320 K, 450 K and above 1000 K
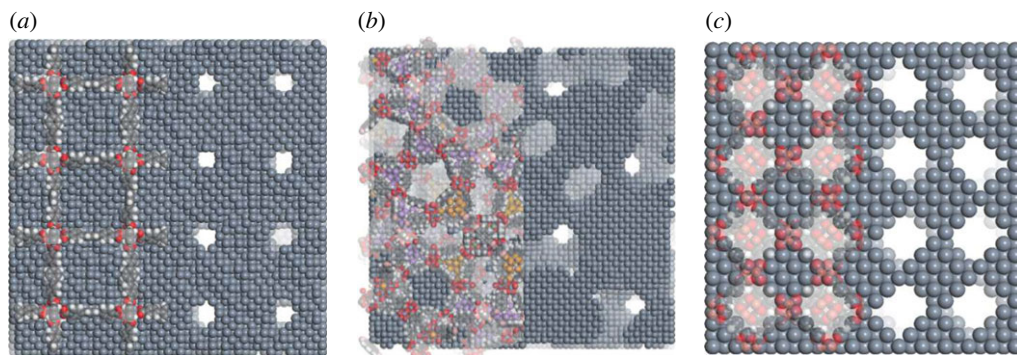
Figure 2. (*a*–*c*) Three of the MOFs structures used as templates, namely IRMOF-16, NDC-MIL-101 and HKUST-1, from left to right. The left side of each panel shows the template and the initially unrelaxed ONM grown within their pores, and the right side shows the ONM once the templating framework is removed. (Online version in colour.)

for MOF-808, BUT-12 and PCN-777, respectively. This result provides confidence in the validity of our procedure for the *in silico* design of ONMs. We then used this procedure to design and to study the stability of new ONMs, with microporous pores (from 0.2 to 2 nm). Materials with such features would exhibit not only strong interactions with guest molecules or ions, but also high densities of sites in direct contact between diffusing species and the solid.

In the absence of any previous knowledge of the factors that control the stability of this family of porous materials, as advanced in the previous section, we first perform a study with the experimentally employed Pt and Pd, with the addition of two related metals, Au and Ag. By doing so, we expect to have data for comparison that allows rationalizing the effect of the nature of the constituent metals. Eight large-pore MOFs, with three-dimensional pore connectivity, were selected for the study: MIL-100 [40], MIL-101 [41], NDC-MIL-101 [42], HKUST [43], MOF-5 [44], IRMOF-16 [45], PCN6P [46] and MOF-500 [47].

Since MIL-101 is a highly robust material, the isoreticular, pore expanded solid that is built with the naphthalenedicarboxylate ligand was also considered, although this structure, with larger pores, would give rise to a lower porosity of the templated ONM. However, we did not know in advance which porosity will be needed for ONMs to be stable, so we also added two series of isoreticular solids to gain insight into the relation between porosity and the stability of ONMs, to do which we employed isoreticular ST solids. In ST materials, each single tetrahedral (T, e.g. T = Si, Ge) node of a topological template structure, like a zeolite, for example, is replaced by an entire larger tetrahedral node [18]. If a tetrahedral atom in the original zeolite structure is replaced by a TX_4 tetrahedron (e.g. X = O, S, Se), a second level supertetrahedral solid (ST2) is formed. Subsequent replacements lead to higher level supertetrahedral solids, e.g. ST3, ST4 and ST5. We built GeS_2 supertetrahedral solids *in silico*, using the Tobunporous code [48,49], which automatically constructs crystalline porous structures, exploiting *in silico* reticular chemistry, based on any desired topology used as topological structural template and rescaling appropriately the cell parameters. An example of a supertetrahedral solid built in this way is shown in figure 1, while in figure 2 we show three of the solids built by templating with MOFs. More snapshots of the stable ONMs are shown in electronic supplementary material, figure S6 of the ESI.

(b) Structural relaxation and analysis of stability

Once all the targeted ONMs solids were designed *in silico*, the structures were subjected to an analysis of their structural features and their stability. We focused on the influence that the level of porosity has on their thermo-structural stability. The as-generated structures were firstly subjected
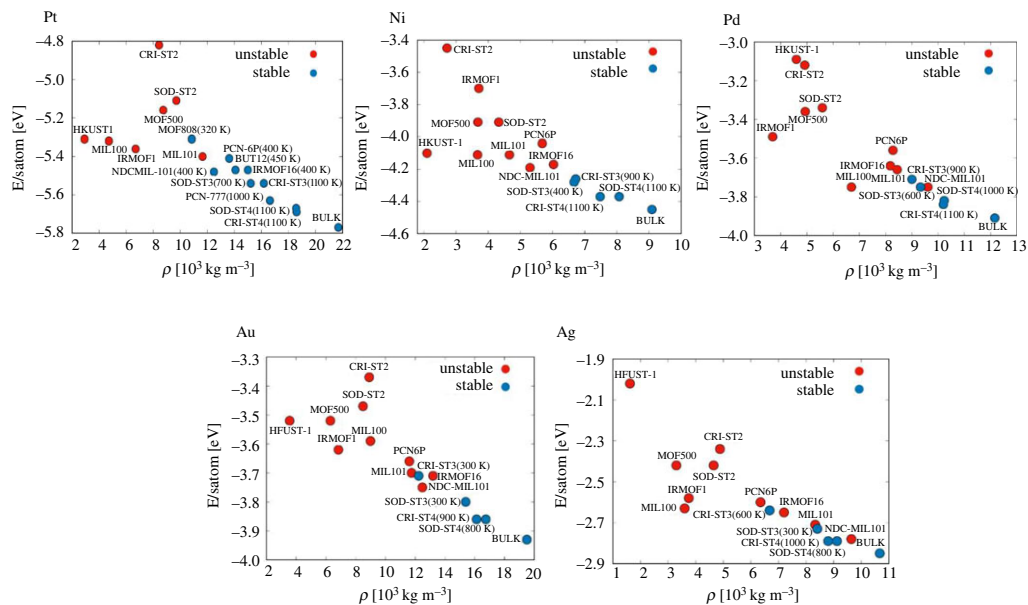
Figure 3. Energy per atom versus density, for all structures studied. Stable structures, in blue, are accompanied by the highest temperature at which they are stable. Structures in red are not stable. (Online version in colour.)

to a lattice energy minimization to relax the solids, which removed the large, initial forces, originating at the low coordinated atoms. Then, long MD simulations (100 ns) were performed as part of the analysis of the stability of the structures.

The stability of the ONM frameworks is shown in figure 3, where ONMs built using Ni are also displayed. The reason for the inclusion of this metal is explained below. We have plotted the energy per atom versus the density of the ONMs, something that is typically performed in other families of porous materials. This plot indicates the possibility of synthesizing a particular structure, comparing the relative energy of the hypothetical materials with respect to that of the most stable structure phase of the material (in our case the bulk metal). This scheme has been useful to predict the structural stability of nanoporous solids, [48–50] like very complex polyoxometalate-based MOFs, which have been successfully synthesized [51]. In figure 3, those structures that are stable after 100 ns of NPT MD simulations are coloured in blue and those that collapse in red. For each stable structure, the higher temperature at which structural stability is maintained is also reported in the figure, in parenthesis. The structures in blue remain porous after long MD simulations, as revealed by their pore size and surface area, ranging from 4.8 to 10.9 Å and 340 to 1500 $m^2\,cm^{-3}$, respectively (see further details in the electronic supplementary material). In figure 3 we see that the stable structures (ONMs that can withstand very high temperatures, even above 1000 K, while keeping their crystallinity intact) can be built from both supertetrahedral solids, with sodalite (SOD-ST3, SOD-ST4) and cristobalite topologies (CRI-ST3, CRI-ST4), and from a number of MOFs structures (NDC-MIL-101, PCN-6P, MOF-500 and IRMOF-16). The cif files of these structures are given as supplementary information. To show that our prediction is robust, we have employed two different potentials in the simulations (see electronic supplementary material, figure S7), which show the same qualitative behaviour in terms of the prediction of which designed ONMs are stable. It is worth noting that our simulation protocol provides structures with accuracy within 2% cell parameters as compared to experiments, e.g. for Pt MOF 808 ONMs these values are 35.2 Å versus 34.5 Å, respectively.

From the analysis of ONMs built with noble metals, Pt ONMs are the best candidates for the experimental preparation with various topologies. Au and Ag ONMs show low stability

since only ST3 and ST4 ONMs of these metals are stable at room temperatures or above. The low stability of Au- and Ag-based ONMs can be ascribed to the ease with which metal surface displacements can take place. From a macroscopic viewpoint, this resembles lateral deformations of the bulk solids, with some atomic layers displacing one on top the other. It is not possible to directly link displacements of metal atoms at the surface to elastic constants, but we can use this information as another qualitative tool to gauge the endurance of the frameworks facing lateral deformations. To analyse this hypothesis, exploiting the cubic symmetry of the parent solids, we calculate the C_{44} elastic constants, which characterize shear deformations [52], and it was found that the highest values are those for Pt and Pd structures. On the other hand, Au and Ag have the smaller values for these elastic constants. For example, in the case of the structure SOD-ST3, C_{44} for Pd and Pt are circa 40 GPa, while it dropped to 20 GPa for Au and Ag. For the sake of comparison, the C_{44} values computed with the potentials for the bulk Pt, Pd, Ag and Au metals are 81.9, 90.5, 51.2 and 51.5 GPa, respectively, which are in good qualitative agreement with those measured experimentally: 77, 71, 51 and 45 GPa [53–57], respectively. We can thus be confident that the new predicted Pd and Pt materials could withstand significant shear deformations. This observation has led us to hypothesize that a low-cost transition metal with FCC crystal structure, as is the case with noble metals, but with higher value of the C_{44} shear elastic constant, could be a good candidate to build ONMs. The experimental C_{44} of bulk Ni, 132 GPa (125.7 GPa when computed with the potentials), is 70% higher than that of Pt, but the price of Ni is three orders of magnitude lower than those of the noble metals. The SOD-ONMs constructed with Ni exhibit a C_{44} value of 60 GPa, that is 50% higher than that of the Pt one. Figure 3 shows that, indeed, a number of ONMs built with Ni are stable. Taking into account our predictions for the five metals studied, and considering the experimental results of Gao *et al.* [3], who were able to prepare Pd, Pt and Rh ONMs, we can conclude that Ni-based ONMs are good candidates for experimental synthesis, as we have found similar stabilities in Pt, Pd and Ni ONMs. To further support the probability of success in the synthesis of low-cost ONMs based on Ni, we confirmed the same behaviour shown in figure 3 using an alternative potential [24] (see electronic supplementary material, figure S7a). Following the work by Gao *et al.* [3] in noble metals, and the amassed experiences on growing Ni structures within porous materials, the predicted stable Ni-ONMs could be prepared. For example, Chemical Vapor Deposition (CVD) methods have already been used by introducing a flow of gaseous nickel tetracarbonyl molecules, $Ni(CO)_4$ [58], which due to their low boiling point (43°C) can enter the large pores of the structures, in the gas phase. They can be decomposed into elemental nickel and CO upon heating [58] to temperatures of circa 200°C, a process that can be repeated in consecutive cycles until the MOF or supertetrahedral host is filled with metallic Ni. Although Ni-nanostructures are known to exist [59–62], and they are used in catalysis and electrochemistry, it is expected that some degree of oxidation [63] would take place, which would hinder their wide use. But there are alternatives that could make unoxidized Ni-based ONMs more stable. For instance, Ni-based superalloys (such as Inconels) are very stable, being used for example in nuclear reactors [64], and thus the predicted Ni-ONMs could be used either as monometal nanostructures or, to minimize oxidation, they can be alloyed to generate robust materials.

Another relevant piece of information arising from figure 3 is the existence of a limiting density (for instance a density of *ca* 10–12 10^3 kg m^{-3} in the case of Pt), below which ONMs are unstable or weakly stable. To put this into perspective, we can analyse the density of zeolites. Stable ONMs densities are *ca* 50% lower than those of their dense counterparts, i.e. bulk metals, while the densities of silica zeolites are in the relative range 46–66% with respect to quartz, the corresponding dense material. Hence, this figure provides additional information to suggest that these materials are thermally stable, and strongly encourages the feasibility of their synthesis, since the difference in energy between the most stable, bulk structures and the porous structures is of the same order of magnitude as that observed in zeolites [50]. As mentioned above, zeolites are metastable structures as compared to their dense counterpart, quartz, but they are, nevertheless, very stable materials, as we see for example in natural zeolites [19]. It is worth noting that the energy differences between the porous, metastable structures and the corresponding stable, dense

structures are in the same range for ONMs and zeolites, but this does not necessarily mean that ONMs have such long metastabilities as zeolites show, since, as mentioned above, the stability of the porous structures is determined by the free energy barriers, which are larger in zeolites, due to their directional covalent bonds, than in ONMs. Based on our simulation method, validated against experimental results, the templating materials CRI-ST4 and SOD-ST4 using Pd or Pt or Ni are expected to give rise to stable ONMs, so they might be the good options when trying to synthesize more members of this new family of porous materials. Moreover, it would be possible to introduce a controlled percentage of other metals in order to increase the hardness of the materials, using the well-known method of solid-solution hardening. The introduction of other metal species could also help to tune the catalytic properties of the materials.

As mentioned above, zeolites and MOFs are metastable materials with respect to the dense polymorphs [48,50,51,65,66], but they show long-lived metastability, which allows their use in applications, even at high pressures and temperatures. We expect a similar behaviour in ONMs, whose stability would be closely related to the energy barrier for atomic diffusion on the internal surface, since a high energy barrier will be responsible for preventing an initial local collapse and eventually the collapse of the whole structure. We studied the energy barriers for atomic diffusion by calculating the free energy profiles for atomic migrations through relevant paths in these materials. The energy profiles are displayed in figure 4, while examples of atomistic views of the diffusion paths are shown in electronic supplementary material, figure S2. The main attention will be focused on the height of the free energy barrier for diffusion, which corresponds to the height of the peak at the right side of the first energy well. This energy is mainly related to that need to remove an atom from its stable position, while the energies of the subsequent barriers are mainly caused by the surface diffusion of this extracted atom and its associated local structural relaxation.

To provide an atomistic insight into the relation between stability and free energy profile for atomic diffusion, Pt-CRI-ST3 was selected among the stable ONMs, since, according to figure 3, it appears in the boundary region that delimits stable and unstable solids. We computed the energy barriers for the two main atomic environments appearing in the internal surfaces of ONMs, namely: flat (figure 4a,e and i for Ni, Pt and Au, respectively) and corner sites (figure 4b,f,j). To facilitate the analysis, an atomistic view of each configuration is shown on the top of figure 4. We see that the energy barriers are environment dependent, which might help explain why some structures are more stable than others, and also the appearance in figure 3 of unstable structures built Pt and Pd. The key result of these calculations is the magnitude of the computed energy barriers corresponding to the unfavourable positions with respect to the stability of the ONM (the corner sites, figure 4b,f,j), as indeed we found that there are high free energy barriers, of 0.89 ± 0.01 eV, 0.88 ± 0.01 and 0.87 ± 0.01 eV for Ni, Pt and Au, respectively, which are close to those observed in the Au (100) surface (a stable surface even in nanoparticles [67]). The observed high values of the energy barriers suggest that, indeed, the ONMs identified in figure 3 as stable are expected to reside in long-lived metastable states, in agreement with the experimental results, which show that there are some Pt and Pd ONMs prepared in the laboratory. The corresponding energy barriers on the flat sites of the ONMs are much higher: 1.84 eV, 1.83 eV and 1.39 eV, respectively.

To have a rationale of the values obtained for the free energy profiles for atomic diffusion on the internal surface of ONMs, a comparison is made conducting the same above analysis on the stable (100) (figure 4c,g,k) and (111) metal surfaces (figure 4d,h,l). The energy barriers for extracting an atom from the Ni, Pt and Au bulk metal surfaces are much higher: 2.03 eV, 2.81 eV and 1.71 eV for the 100 surface, and 2.24 eV, 2.87 eV and 1.71 eV for the (111) surface. It can be also observed that the free energy profiles of moving one already extracted atom on these two surfaces is very different, once the relative depths of the second energy well in figure 4c,d,g,h,k,i, are for the (111) surfaces at least half of those of the (100) ones. This agrees with calculations carried out by Crljen et al. [68]. In all cases, the energy barriers for Au are lower than for Ni or Pt. This agrees with the overall lower stability of Au ONMs observed in figure 3. To help rationalize this point we have added the radial distribution function in each case to the top axis of figure 4. The first
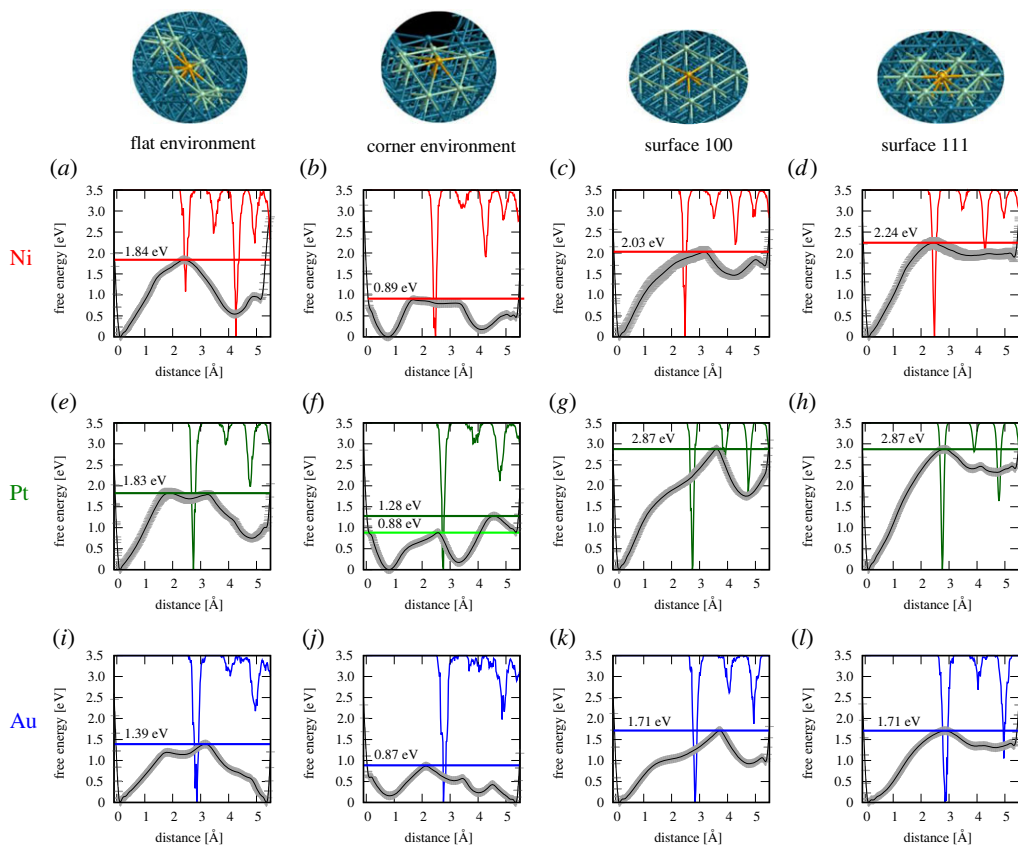
Figure 4. Free energy profiles (including error bars) of a biased metal atom moving on a material surface, calculated by NPT MetaD simulations for Ni (*a*–*d*), Pt (*e*–*h*) and Au (*i*–*l*) atoms, in four types of environments: flat environment of the internal surface of CRI-ST3 ONM (subfigures *a*, *e* and *i*), corner environment of the internal surface of CRI-ST3 ONM (subfigures *b*, *f* and *j*), bulk metal surface (111) (subfigures *c*, *g* and *k*), and (100) surface (subfigures *d*, *h* and *l*). In the top of the panel there are four snapshots of each environment. We have plotted for each system (metal and environment) the radial distribution function, *g*(*r*), between the moving metal atom and the closest neighbour (5.5 Å) in an NPT MD equilibration simulation (when the moving particle is not yet biased). The colours in the *g*(*r*) are red, green and blue for Ni, Pt and Au atoms, respectively. The atom colour code for the structural snapshots is the following: in yellow the moving metallic atom, in green the defined nest-type environment, and in blue the rest of the metallic atoms of the corresponding material. For each system, the jumping free energy barriers are shown. (Online version in colour.)

peak corresponds to the next-neighbour distances. The larger Au-Au interatomic distances can be a factor behind the weakness observed in Au-ONMs, as they might have a large effect on the cohesion, particularly at low local density regions.

To investigate whether it would be possible to predict the stability of OMNs from structural descriptors of a given MOF or ST solid, we analyse the porosity and textural properties of the 17 solids used here as hard-sacrificial templates. We have focused on Pt-ONMs, considering their successful experimental synthesis and the theoretical results that identify this element as one with which to create stable hypothetical ONMs. Due to the limited amount of data to compare with, we do not aim to have a fine quantitative prediction, but a semiquantitative one that could help synthesis efforts and to stimulate further work in this direction. Among the structural descriptors, we found a significant relation between the stability of the predicted ONMs and the pore limiting diameter (PLD) of the template structures. The PLD is defined as the largest diameter that a sphere can have within the framework, so that it can move through the structure without overlapping any framework atom. It is a measure of how large the pore entrance is, and consequently, will
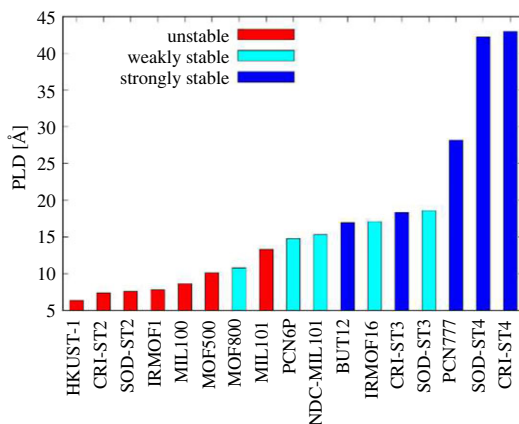
Figure 5. Pore limiting diameters (PLDs) of Pt-based ONMs, for the 17 different topologies investigated. (Online version in colour.)

determine how thick the templated metal wall or column can be. We found that the PLDs of the predicted stable ONMs (figure 5) are in the range [14.76 Å, 42.96 Å], while for the unstable ONMs they are within the range [6.37 Å, 13.31 Å]. The PLDs of the three experimental structures templated with MOFs (synthesized by Gao *et al.* [3]) are 10.80 Å (from MOF-808), 16.94 Å (from BUT-12) and 28.17 Å (from PCN-777). The two latter lie in the interval we predicted for the stable ONMs, while the PLD of MOF-808 is smaller than that of the unstable MIL-101. To rationalize this apparent controversy, we must note that MIL-101 has two types of pores. The PLD (approx. 15 Å) is given by hexagonal windows delimiting the entrance to the larger pores, while the smaller diameter (approx. 10 Å) corresponds to pentagonal windows delimiting the smaller pores. This is a space that can be occupied by metal atoms, but it does not yield a robust enough structure, as in the case of MOF-500, which has a PLD of 10.12 Å.

We can then state that the collapse of the smaller metal units formed at the smaller and more numerous pentagonal windows of the MIL-101 will trigger the collapse of the whole material. This resembles the collapse of some MOFs upon desolvation of strong interacting solvents, triggered by capillary forces [69] and the chemical welding and sintering of metallic nanostructures at room temperature [70]. Note that the isoreticular MOF NDC-MIL-101, with pore windows that are 15% larger, does form a stable ONM. The appearance of a minimum value of PLD of the template porous solids as a requisite for preparing stable ONMs is in line with our view of lateral internal surface atomic diffusion as the key-point controlling the stability of ONMs. In principle, our finding is valid only for those templating structures that render metal columns or walls thicker than that corresponding to the negative image of the critical PLD. Considering the limitation of the experimental and theoretical data, using Pt as a reference and proposing that the other FCC metals would behave in a similar way, we propose as a rough estimate that the critical PLD (PLD$_c$) of a porous host that yielded stable ONMs can be empirically described by the following equation (see electronic supplementary material for details of how this equation was derived and for additional data about porosities): PLD$_c = 2R_{vdw} + 7.5R_{atom}$, where R_{vdw} and R_{atom} are the van der Waals and atomic radii, respectively, of the ONM-constituent metal. The largest cavity diameter (LCD) of the template host solids does not play a significant role in the stability of the ONMs, and neither do the accessible surface area and the accessible helium void fraction. Details of the computed porosity and textural properties are reported in the electronic supplementary material.

Since these materials are likely to be used in applications at which there are significant changes in temperature, we have also studied their thermal behaviour. In figure 6 we show the results obtained from the analysis of the heat capacities, calculated from MD simulations. The computed values for five out of the seven solids lay close to those of the bulk structures. A slight departure
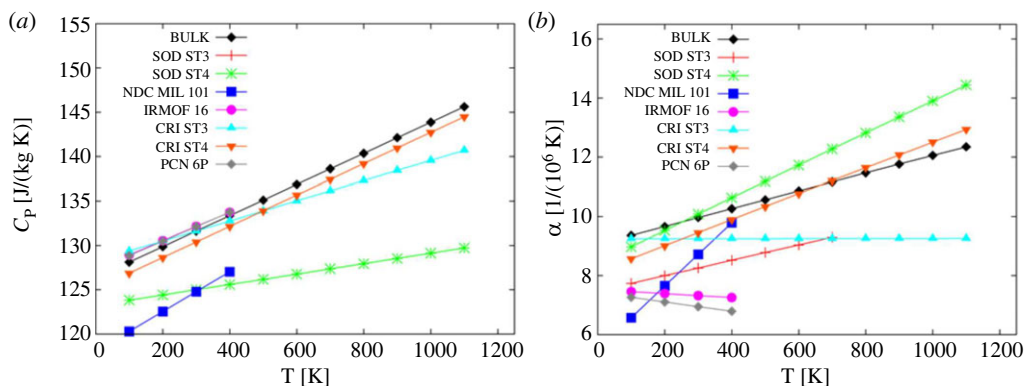
Figure 6. Specific heat (*a*) and volumetric thermal expansion coefficient (*b*), and for the ONMs generated with platinum and modelled with the interatomic potential developed by Sheng *et al.* [23]. The final temperatures for each structure are those at which each material collapses. (Online version in colour.)

is observed for CRI-ST3 ONM, and large differences appeared for NDC-MIL-101 and SOD-ST4 ONMs. We did not find any direct connection between the structure of these solids and the computed heat capacity behaviour with temperature.

The thermal expansion (also shown in figure 6) also appears to be uncorrelated. The calculated values span over a wide range, with one solid unexpectedly showing nearly zero thermal expansion (CRI-ST3 ONM) and two with negative thermal expansion (IRMOF-16 and PCN6P ONMs). To our knowledge, zero and negative thermal expansions have not been predicted before for nanoporous solids built by one elemental metal. The open framework nature of these solids could be the reason behind this uncommon behaviour, which frequently occurs in traditional microporous solids, such as zeolites [71,72] and MOFs [49,73,74], and also non-porous framework materials like ZrW_2O_8 and quartz [75]. This interesting finding might open a new area of research in the field of thermal structural materials.

(c) Transport properties of guest molecules

Evaluating the performance of new metallic nanostructured solids, as for instance shown in metal nanoparticles or nanorods supported on different materials [76,77], is still crucial for several applications. In order for the designed ONMs to be used in separation, molecular-enhanced heat exchange, catalysis or highly molecular-permeable electrode in electrochemistry applications, the stable structures should be able to allow the flow of molecules at a rate comparable to other microporous solids. We, therefore, computed the diffusion coefficients of four relevant molecules (benzene, o-xylene, m-xylene and p-xylene), within the Ag-CRI-ST3 structure, and the diffusion of water and methanol within the structures Pt-CRI-ST3, Pt-PCN-6P and NDC-MIL-101 (table 1).

From the data shown in table 1 we can conclude that, since diffusion coefficients are of the order of $10^{-9}\,\mathrm{m^2\,s^{-1}}$, which is of the same order of magnitude as for diffusion in zeolites [78], and MOFs [79,80], these materials could have the required flow of molecules to allow their use in some relevant industrial applications, for example in green sustainable production of fuels and chemical feedstocks and in petro-chemistry. For instance, if we compare the diffusion coefficients at 300 K of benzene and the three xylene isomers in the silver Ag-CRI-ST3 structure, we observe that benzene diffusion is much faster than that of xylenes, and also it can be noted that the isomers diffuse at slightly different rates, so this structure could be used to separate mixtures of these molecules (table 1). To see if there is an enthalpic ground for the observed behaviour, we turned to the calculation of the heat of adsorption of these molecules on this material and on the Ag (100) and (111) surfaces, obtained with Monte Carlo

Table 1. Self-diffusion coefficients, D_s, $\triangle H_{ads}$ for benzene, o-xylene, m-xylene, p-xylene, water and methanol molecules in various Ag-, Pt- and Ni-based ONMs, calculated with MD-NVT simulations at 298.15 K. Mixing rules are used to obtain the force field parameters between host and guest.

metal	ONM (force field Ref.)	molecule (force field Ref.)	D_s (10^{-9} m^2 s^{-1})
Ag	CRI ST3[a]	benzene[d]	1.5
		orthoxylene[d]	0.20
		metaxylene[d]	0.46
		paraxylene[d]	0.32
Pt	CRI ST3[b]	methanol[d]	1.4
		water[e]	1.1
	PCN 6P[b]	methanol[d]	1.4
		water[e]	1.3
	NDC MIL 101[b]	methanol[d]	1.4
		water[e]	1.6
Ni	CRI ST3[c]	water[e]	0.74
		methanol[d]	0.20

[a] Jalkanen & Zerbetto [35].
[b] Tarmyshov & Müller-Plathe [36].
[c] Heinz et al. [37].
[d] Mayo et al. [34].
[e] Price & Brooks (TIP3P) [33].

calculations (electronic supplementary material, figure S8). We can get some degree of confidence on the validity of the calculations, by comparing the experimental [81] value of adsorption enthalpy of benzene over the Ag(111) surface, -40 kJ mol^{-1}, with the values obtained in our calculations, -46 kJ mol^{-1}. We see that there is a stronger adsorption within the Ag CRI-ST3 pores than on the metal surfaces. For instance, the enthalpy of adsorption of the xylene isomers is circa -70 kJ mol^{-1} within the pores, while it is -51 kJ mol^{-1} on the Ag(100) surface and -55 kJ mol^{-1} on the Ag(111) surface. The differences in the diffusion coefficients of the three xylenes seem to be caused by entropic effects associated with the geometry differences between these molecules, rather than being originated by enthalpic effects [82]. The important point to note is that confinement does have a significant effect, and given the large number of possible topologies, there should be an ONM in which significant separation would occur. Although very interesting, this exploration falls out of the scope of the present study and will be a matter of forthcoming research. Also, in future work, the effect of chemisorption within ONMs will be studied, since it is known that the presence of foreign atoms on Ni, e.g. Al, could give rise to water chemisorption through the formation of Al_2O_3 at the surfaces [83]. This process is not simulated here, as the formation of metal oxides layers are not considered due to the nature of the studied metals.

The overall lack of correlation between thermal expansion, heat capacity, diffusion coefficients textural properties and structural features does not mean that these correlations do not exist. In future work, once a large number of ONMs is available, this topic will be analysed in depth, using machine learning methods to identify the key correlations, if present. In addition, further insight into the catalytic performance would be gained by that analysis. The expected defective nature of ONMs, as well as their use along with supported catalysts, would induce strain and more diversity of sites, which could incorporate richness into their catalytic and sorption performance, as has been observed in some nanostructured materials [84,85]. These are new avenues that remain open for future work.

4. Conclusion

To summarize, the stability and structural properties of the recently discovered family of ordered nanoporous metals (ONMs) have been studied, which has resulted in guidelines for stimulating further synthetic work. In doing so, we have developed an *in silico* strategy for the design of stable ONMs that is validated by reproducing the structure of the experimentally known materials. The long-lived nature of these structures has been addressed by combining molecular dynamics and metadynamics-based free energy barrier calculations, to investigate the primary stage of materials degradation. We have shown that besides MOFs, which were previously used in the pioneering work of this novel family of solids, supertetrahedral solids can also be used as reverse templates for growing their 'negative' replica metal structures. Some of the ordered metal structures thus formed are predicted to withstand temperatures as high as 1000 K. We rationalize the stability of the ONMs based on the porosity of the parent material and the nature of the shear elasticity of the constituent metal of the metallic nanostructure. We have found that the PLDs of the template hosts can be used as a preliminary descriptor for selecting potential porous materials that would give rise to stable ONMs. Learning from the study of ONMs built by noble metals, we have predicted stable low-cost ordered nanoporous metals (ONMs) based on Earth-abundant Ni metal, about a thousand times less expensive than existing Pt, Pd and Rh materials, and consequently they are expected to spread in a wide range of advanced applications in molecular sieving, catalysis and electrochemistry, with particular impact when the coexistence of the three scenarios exists. We also found negative and zero thermal expansion in some of the studied solids, which can open new research directions in the structural materials area. Due to the high surface area of these structures, the most relevant applications are expected to be in the fields of separation and catalysis, particularly in thin membrane technologies where the molecular sieving features can be combined with high thermal and chemical stabilities, as well as the high electronic conductivity intrinsically associated with metallic materials. The later also opens space for their use as advanced electrodes in batteries and fuel cells. As a prerequisite for such applications, we have shown the feasibility of molecular diffusion of molecules representative of those used in renewable and traditional fuels industries. Our approach can lead to the prediction of a library of hypothetical ONMs that can shed light on the hitherto hidden relationships between properties such as porosity, pore size, pore limiting diameter, thermal expansion or self-diffusion coefficients. This will be a next step in predicting ONMs for advanced applications and could further stimulate their experimental study.

Authors' contributions. J.M.O.-R.: conceptualization, data curation, formal analysis, investigation, methodology, writing—original draft, writing—review and editing; S.R.G.B.: conceptualization, formal analysis, investigation, methodology, software, validation, visualization, writing—original draft, writing—review and editing; R.B.-P.: formal analysis, investigation, writing—review and editing; S.C.: funding acquisition, investigation, project administration, writing—original draft, writing—review and editing; E.G.-P.: formal analysis, investigation, writing—review and editing; C.R.A.C.: conceptualization, formal analysis, investigation, supervision, writing—original draft, writing—review and editing; A.R.R.-S.: conceptualization, investigation, methodology, supervision, writing—original draft, writing—review and editing; S.H.: conceptualization, investigation, methodology, supervision, writing—original draft, writing—review and editing.

All authors gave final approval for publication and agreed to be held accountable for the work performed therein.

References

1. Luc W, Jiao F. 2016 Synthesis of nanoporous metals, oxides, carbides, and sulfides: beyond nanocasting. *Acc. Chem. Res.* **49**, 1351–1358. (doi:10.1021/acs.accounts.6b00109)
2. Thomas JM. 2018 The enduring relevance and academic fascination of catalysis. *Nat. Catal.* **1**, 2–5. (doi:10.1038/s41929-017-0014-0)
3. Gao X *et al.* 2019 Casting nanoporous platinum in metal–organic frameworks. *Adv. Mater.* **31**, 1807553. (doi:10.1002/adma.201807553)
4. Ma Z, Kyotani T, Tomita A. 2000 Preparation of a high surface area microporous carbon having the structural regularity of Y zeolite. *Chem. Commun.* 2365–2366. (doi:10.1039/b006295m)
5. Nugraha AS, Lambard G, Na J, Hossain MSA, Asahi T, Chaikittisilp W, Yamauchi Y. 2020 Mesoporous trimetallic PtPdAu alloy films toward enhanced electrocatalytic activity in methanol oxidation: unexpected chemical compositions discovered by Bayesian optimization. *J. Mater. Chem. A* **8**, 13 532–13 540. (doi:10.1039/d0ta04096g)
6. Chen Q, Ding Y, Chen M. 2018 Nanoporous metal by dealloying for electrochemical energy conversion and storage. *MRS Bull.* **43**, 43–48. (doi:10.1557/mrs.2017.300)
7. Fujita T. 2017 Hierarchical nanoporous metals as a path toward the ultimate three-dimensional functionality. *Sci. Technol. Adv. Mater.* **18**, 724–740. (doi:10.1080/14686996.2017.1377047)
8. Tappan BCCB, Steiner SAAS, Luther EPP. 2010 Nanoporous metal foams. *Angew. Chem. Int. Ed. Engl.* **49**, 4544–4565. (doi:10.1002/anie.200902994)
9. Fujita T. 2019 Diversity of nanoporous metals. *Metals (Basel)* **9**, 7–8. (doi:10.3390/met9090996)
10. Koya AN, Zhu X, Ohannesian N, Yanik AA, Alabastri A, Proietti Zaccaria R, Krahne R, Shih WC, Garoli D. 2021 Nanoporous metals: from plasmonic properties to applications in enhanced spectroscopy and photocatalysis. *ACS Nano.* **15**, 6038–6060. (doi:10.1021/acsnano.0c10945)
11. Qiu HJ, Li X, Xu HT, Zhang HJ, Wang Y. 2014 Nanoporous metal as a platform for electrochemical and optical sensing. *J. Mater. Chem. C.* **2**, 9788–9799. (doi:10.1039/c4tc01913j)
12. Braun E, Lee Y, Moosavi SM, Barthel S, Mercado R, Baburin IA, Proserpio DM, Smit B. 2018 Generating carbon schwarzites via zeolite-templating. *Proc. Natl Acad. Sci. USA* **115**, E8116–E8124. (doi:10.1073/pnas.1805062115)
13. Wu J, Zhang K, Yoo H, Lee Y. 2022 *In silico* generation of a topologically diverse zeolite-templated carbon library. *Cryst. Growth Des.* **22**, 123–130. (doi:10.1021/acs.cgd.1c00620)
14. Roussel T, Didion A, Pellenq RJM, Gadiou R, Bichara C, Vix-Guterl C. 2007 Experimental and atomistic simulation study of the structural and adsorption properties of faujasite zeolite-templated nanostructured carbon materials. *J. Phys. Chem. C* **111**, 15 863–15 876. (doi:10.1021/jp0746906)
15. Roussel T, Jagiello J, Pellenq RJM, Thommes M, Bichara C. 2006 Testing the feasibility of using the density functional theory route for pore size distribution calculations of ordered microporous carbons. *Mol. Simul.* **32**, 551–555. (doi:10.1080/08927020500517231)
16. Nishihara H *et al.* 2009 A possible buckybowl-like structure of zeolite templated carbon. *Carbon N. Y.* **47**, 1220–1230. (doi:10.1016/j.carbon.2008.12.040)
17. Nishihara H *et al.* 2018 Graphene-based ordered framework with a diverse range of carbon polygons formed in zeolite nanochannels. *Carbon N. Y.* **129**, 854–862. (doi:10.1016/j.carbon.2017.12.055)
18. Lin Q, Bu X, Mao C, Zhao X, Sasan K, Feng P. 2015 Mimicking high-silica zeolites: highly stable germanium- and tin-rich zeolite-type chalcogenides. *J. Am. Chem. Soc.* **137**, 6184–6187. (doi:10.1021/jacs.5b03550)

19. Gottardi G. 1989 The genesis of zeolites. *Eur. J. Mineral.* **1**, 479–488. (doi:10.1127/ejm/1/4/0479)

20. Lee P, Lee J, Lee H, Yeo J, Hong S, Nam KH, Lee D, Lee SS, Ko SH. 2012 Highly stretchable and highly conductive metal electrode by very long metal nanowire percolation network. *Adv. Mater.* **24**, 3326–3332. (doi:10.1002/adma.201200359)

21. Lee H, Kim K, Kang SH, Kwon Y, Kim JH, Kwon YK, Ryoo R, Park JY. 2017 Extremely high electrical conductance of microporous 3D graphene-like zeolite-templated carbon framework. *Sci. Rep.* **7**, 1–9. (doi:10.1038/s41598-017-11602-5)

22. Plimpton S. 1995 Fast parallel algorithms for short-range molecular dynamics. *J. Comput. Phys.* **117**, 1–19. (doi:10.1006/jcph.1995.1039)

23. Sheng HW, Kramer MJ, Cadien A, Fujita T, Chen MW. 2011 Highly optimized embedded-atom-method potentials for fourteen FCC metals. *Phys. Rev. B - Condens. Matter Mater. Phys.* **83**, 1–20. (doi:10.1103/PhysRevB.83.134118)

24. Ortiz-Roldan JM, Ruiz-Salvador AR, Calero S, Montero-Chacón F, García-Pérez E, Segurado J, Martin-Bragado I, Hamad S. 2015 Thermostructural behaviour of Ni–Cr materials: modelling of bulk and nanoparticle systems. *Phys. Chem. Chem. Phys.* **17**, 15 912–15 920. (doi:10.1039/C5CP01785H)

25. Gan Y, Sun Z, Chen Z. 2015 Extensional vibration and size-dependent mechanical properties of single-crystal gold nanorods. *J. Appl. Phys.* **118**, 164 304-1–164 304-5. (doi:10.1063/1.4934643)

26. Da Silva EZ *et al.* 2019 Connecting theory with experiment to understand the sintering processes of Ag nanoparticles. *J. Phys. Chem. C.* **123**, 11 310–11 318. (doi:10.1021/acs.jpcc.9b02107)

27. Patil RP, Doan D, Aitken ZH, Chen S, Kiani MT, Barr CM, Hattar K, Zhang YW, Gu XW. 2020 Hardening in Au-Ag nanoboxes from stacking fault-dislocation interactions. *Nat. Commun.* **11**, 1–9. (doi:10.1038/s41467-020-16760-1)

28. Laio A, Parrinello M. 2002 Escaping free-energy minima. *Proc. Natl Acad. Sci. USA* **99**, 12 562–12 566. (doi:10.1073/pnas.202427399)

29. Barducci A, Bussi G, Parrinello M. 2008 Well-tempered metadynamics: a smoothly converging and tunable free-energy method. *Phys. Rev. Lett.* **100**, 20603. (doi:10.1103/PhysRevLett.100.020603)

30. Colón-Ramos DA, La Riviere P, Shroff H, Oldenbourg R. 2019 Transforming the development and dissemination of cutting-edge microscopy and computation. *Nat. Methods* **16**, 667–669. (doi:10.1038/s41592-019-0475-y)

31. Tribello GA, Bonomi M, Branduardi D, Camilloni C, Bussi G. 2014 PLUMED 2: new feathers for an old bird. *Comput. Phys. Commun.* **185**, 604–613. (doi:10.1016/j.cpc.2013.09.018)

32. Tribello GA, Giberti F, Sosso GC, Salvalaglio M, Parrinello M. 2017 Analyzing and driving cluster formation in atomistic simulations. *J. Chem. Theory Comput.* **13**, 1317–1327. (doi:10.1021/acs.jctc.6b01073)

33. Price DJ, Brooks CL. 2004 A modified TIP3P water potential for simulation with Ewald summation. *J. Chem. Phys.* **121**, 10 096–10 103. (doi:10.1063/1.1808117)

34. Mayo SL, Olafson BD, Goddard WA. 1990 DREIDING: a generic force field for molecular simulations. *J. Phys. Chem.* **101**, 8897–8909. (doi:10.1021/j100389a010)

35. Jalkanen JP, Zerbetto F. 2006 Interaction model for the adsorption of organic molecules on the silver surface. *J. Phys. Chem. B* **110**, 5595–5601. (doi:10.1021/jp055225g)

36. Tarmyshov KB, Müller-Plathe F. 2007 Interface between platinum(111) and liquid isopropanol (2-propanol): a model for molecular dynamics studies. *J. Chem. Phys.* **126**, 074702. (doi:10.1063/1.2472357)

37. Heinz H, a Vaia R, Farmer BL, Naik RR. 2008 Accurate simulation of surfaces and interfaces of face-centered cubic metals using 12- 6 and 9- 6 Lennard-Jones potentials. *J. Phys. Chem. C* **112**, 17 281–17 290. (doi:10.1021/jp801931d)

38. Dubbeldam D, Calero S, Ellis DE, Snurr RQ. 2015 RASPA: molecular simulation software for adsorption and diffusion in flexible nanoporous materials. *Mol. Simul.* **42**, 1–21. (doi:10.1080/08927022.2015.1010082)

39. Sarkisov L, Harrison A. 2011 Computational structure characterisation tools in application to ordered and disordered porous materials. *Mol. Simul.* **37**, 1248–1257. (doi:10.1080/08927022.2011.592832)

40. Férey G, Serre C, Mellot-Draznieks C, Millange F, Surblé S, Dutour J, Margiolaki I. 2004 A hybrid solid with giant pores prepared by a combination of targeted chemistry, simulation, and powder diffraction. *Angew. Chemie Int. Ed.* **43**, 6296–6301. (doi:10.1002/anie.200460592)

41. Férey G, Mellot-Draznieks C, Serre C, Millange F, Dutour J, Surblé S, Margiolaki I. 2005 A chromium terephthalate-based solid with unusually large pore volumes and surface area. *Science* **309**, 2040–2042. (doi:10.1126/science.1116275)

42. Sonnauer A, Hoffmann F, Fröba M, Kienle L, Duppel V, Thommes M, Serre C, Férey G, Stock N. 2009 Giant pores in a chromium 2,6-naphthalenedicarboxylate open-framework structure with MIL-101 topology. *Angew. Chemie Int. Ed.* **48**, 3791–3794. (doi:10.1002/anie.200805980)

43. Chui SSY, Lo SMF, Charmant JPH, Orpen AG, Williams ID. 1999 A chemically functionalizable nanoporous material. *Science* **283**, 1148–1150. (doi:10.1126/science.283.5405.1148)

44. Li H, Eddaoudi M, O'Keeffe M, Yaghi OM. 1999 Design and synthesis of an exceptionally stable and highly porous metal-organic framework. *Nature* **402**, 276–279. (doi:10.1038/46248)

45. Eddaoudi M, Kim J, Rosi N, Vodak D, Wachter J, O'Keeffe M, Yaghi OM. 2002 Systematic design of pore size and functionality in isoreticular MOFs and their application in methane storage. *Science* **295**, 469–472. (doi:10.1126/science.1067208)

46. Ma S, Sun D, Ambrogio M, Fillinger JA, Parkin S, Zhou HC. 2007 Framework-catenation isomerism in metal-organic frameworks and its impact on hydrogen uptake. *J. Am. Chem. Soc.* **129**, 1858–1859. (doi:10.1021/ja067435s)

47. Sudik AC, Côté AP, Wong-Foy AG, O'Keeffe M, Yaghi OM. 2006 A metal–organic framework with a hierarchical system of pores and tetrahedral building blocks. *Angew. Chemie Int. Ed.* **45**, 2528–2533. (doi:10.1002/anie.200600175)

48. Lewis DW, Ruiz-Salvador AR, Gómez A, Rodriguez-Albelo LM, Coudert F-X, Slater B, Cheetham AK, Mellot-Draznieks C. 2009 Zeolitic imidazole frameworks: structural and energetics trends compared with their zeolite analogues. *CrystEngComm* **11**, 2272. (doi:10.1039/b912997a)

49. Burtch NC, Baxter SJ, Heinen J, Bird A, Schneemann A, Dubbeldam D, Wilkinson AP. 2019 Negative thermal expansion design strategies in a diverse series of metal–organic frameworks. *Adv. Funct. Mater.* **29**, 1904669. (doi:10.1002/adfm.201904669)

50. Henson NJ, Cheetham AK, Gale JD. 1994 Theoretical calculations on silica frameworks and their correlation with experiment. *Chem. Mater.* **6**, 1647–1650. (doi:10.1021/cm00046a015)

51. Rodriguez-Albelo LM *et al.* 2009 Zeolitic polyoxometalate-based metal-organic frameworks (Z-POMOFs): computational evaluation of hypothetical polymorphs and the successful targeted synthesis of the redox-active Z-POMOF1. *J. Am. Chem. Soc.* **131**, 16 078–16 087. (doi:10.1021/ja905009e)

52. Kushwaha AK, Khenata R, Bouhemadou A, Bin-Omran S, Haddadi K. 2017 Lattice dynamical properties and elastic constants of the ternary chalcopyrite compounds $CuAlS_2$, $CuGaS_2$, $CuInS_2$, and $AgGaS2$. *J. Electron. Mater.* **46**, 4109–4118. (doi:10.1007/s11664-017-5290-6)

53. Simons G, Wang H. 1977 Single crystal elastic constants and calculated aggregate properties. *J. Gd. Res. Center 1965* **34**, 269.

54. Nye J. 1957 *Physical Properties of Crystals*.

55. Leigh GJ. 1994 Macmillan's chemical and physical data. *J. Organomet. Chem.* **471**, C11–C12. (doi:10.1016/0022-328x(94)88141-3)

56. Kaye GWC, Laby TH. 1921 Tables of physical and chemical contrasts and some mathematical functions. *Math. Gaz.* **10**, 351. (doi:10.2307/3605218)

57. Samsonov GV, Straumanis ME. 1968 Handbook of the physicochemical properties of the elements. *Phys. Today* **21**, 97. (doi:10.1063/1.3035172)

58. Paserin V, Marcuson S, Shu J, Wilkinson DS. 2004 CVD technique for inco nickel foam production. *Adv. Eng. Mater.* **6**, 454–459. (doi:10.1002/adem.200405142)

59. Drisko GL, Gatel C, Fazzini PF, Ibarra A, Mourdikoudis S, Bley V, Fajerwerg K, Fau P, Kahn M. 2018 Air-stable anisotropic monocrystalline nickel nanowires characterized using electron holography. *Nano Lett.* **18**, 1733–1738. (doi:10.1021/acs.nanolett.7b04791)

60. Remadevi A, Kesavapillai Sreedeviamma D, Surendran KP. 2018 Printable hierarchical nickel nanowires for soft magnetic applications. *ACS Omega* **3**, 14 245–14 257. (doi:10.1021/acsomega.8b01422)

61. Pilban Jahromi S, Zareian M, Ming HN, Pei J, Kamalianfar A, Okoro OV, Zhang H. 2021 The effect of supporting electrolyte concentrations on the growth of nickel nanostructures. *J. Alloys Compd.* **880**, 160408. (doi:10.1016/j.jallcom.2021.160408)

62. Ni W, Bin Wu H, Wang B, Xu R, Lou XW. 2012 One-pot synthesis of ultra-light nickel nanofoams composed of nanowires and their transformation into various functional nanofoams. *Small.* **8**, 3432–3437. ([doi:10.1002/smll.201201678](https://doi.org/10.1002/smll.201201678))

63. Cossar E, Houache MSE, Zhang Z, Baranova EA. 2020 Comparison of electrochemical active surface area methods for various nickel nanostructures. *J. Electroanal. Chem.* **870**, 114246. ([doi:10.1016/j.jelechem.2020.114246](https://doi.org/10.1016/j.jelechem.2020.114246))

64. Tsigkis V, Saifur Rahman M, Hackel L, Davami K, Beheshti A, Polycarpou AA. 2022 Helium tribology of Inconel 617 subjected to laser peening for high temperature nuclear reactor applications. *Appl. Surf. Sci.* **577**, 151961. ([doi:10.1016/j.apsusc.2021.151961](https://doi.org/10.1016/j.apsusc.2021.151961))

65. Piccione PM, Laberty C, Yang S, Camblor MA, Navrotsky A, Davis ME. 2000 Thermochemistry of pure-silica zeolites. *J. Phys. Chem. B* **104**, 10001–10011. ([doi:10.1021/jp002148a](https://doi.org/10.1021/jp002148a))

66. Hughes JT, Bennett TD, Cheetham AK, Navrotsky A. 2013 Thermochemistry of zeolitic imidazolate frameworks of varying porosity. *J. Am. Chem. Soc.* **135**, 598–601. ([doi:10.1021/ja311237m](https://doi.org/10.1021/ja311237m))

67. Brown M, Wiley BJ. 2020 Bromide causes facet-selective atomic addition in gold nanorod syntheses. *Chem. Mater.* **32**, 6410–6415. ([doi:10.1021/acs.chemmater.0c01494](https://doi.org/10.1021/acs.chemmater.0c01494))

68. Crljen Ž, Lazić P, Šokčević D, Brako R. 2003 Relaxation and reconstruction on (111) surfaces of Au, Pt, and Cu. *Phys. Rev. B - Condens. Matter Mater. Phys.* **68**, 195411. ([doi:10.1103/PhysRevB.68.195411](https://doi.org/10.1103/PhysRevB.68.195411))

69. Mondloch JE, Katz MJ, Planas N, Semrouni D, Gagliardi L, Hupp JT, Farha OK. 2014 Are Zr6-based MOFs water stable? Linker hydrolysis vs. capillary-force-driven channel collapse. *Chem. Commun.* **50**, 8944–8946. ([doi:10.1039/c4cc02401j](https://doi.org/10.1039/c4cc02401j))

70. Yoon S-S, Khang D-Y. 2016 Room-temperature chemical welding and sintering of metallic nanostructures by capillary condensation. *Nano Lett.* **16**, 3550–3556. ([doi:10.1021/acs.nanolett.6b00621](https://doi.org/10.1021/acs.nanolett.6b00621))

71. Lightfoot P, Woodcock DA, Maple MJ, Villaescusa LA, Wright PA. 2001 The widespread occurrence of negative thermal expansion in zeolites. *J. Mater. Chem.* **11**, 212–216. ([doi:10.1039/b002950p](https://doi.org/10.1039/b002950p))

72. Carey T, Tang CC, Hriljac JA, Anderson PA. 2014 Chemical control of thermal expansion in cation-exchanged Zeolite A. *Chem. Mater.* **26**, 1561–1566. ([doi:10.1021/cm403312q](https://doi.org/10.1021/cm403312q))

73. Liu Z, Gao Q, Chen J, Deng J, Lin K, Xing X. 2018 Negative thermal expansion in molecular materials. *Chem. Commun.* **54**, 5164–5176. ([doi:10.1039/C8CC01153B](https://doi.org/10.1039/C8CC01153B))

74. Balestra SRG, Bueno-Perez R, Hamad S, Dubbeldam D, Ruiz-Salvador AR, Calero S. 2016 Controlling thermal expansion: a metal–organic frameworks route. *Chem. Mater.* **28**, 8296–8304. ([doi:10.1021/acs.chemmater.6b03457](https://doi.org/10.1021/acs.chemmater.6b03457))

75. Fang H, Dove MT, Phillips AE. 2014 Common origin of negative thermal expansion and other exotic properties in ceramic and hybrid materials. *Phys. Rev. B* **89**, 214103. ([doi:10.1103/PhysRevB.89.214103](https://doi.org/10.1103/PhysRevB.89.214103))

76. He L, Weniger F, Neumann H, Beller M. 2016 Synthesis, characterization, and application of metal nanoparticles supported on nitrogen-doped carbon: catalysis beyond electrochemistry. *Angew. Chemie Int. Ed.* **55**, 12582–12594. ([doi:10.1002/anie.201603198](https://doi.org/10.1002/anie.201603198))

77. Ben-Shahar Y, Scotognella F, Kriegel I, Moretti L, Cerullo G, Rabani E, Banin U. 2016 Optimal metal domain size for photocatalysis with hybrid semiconductor-metal nanorods. *Nat. Commun.* **7**, 10413. ([doi:10.1038/ncomms10413](https://doi.org/10.1038/ncomms10413))

78. Chmelik C, Kärger J. 2010 In situ study on molecular diffusion phenomena in nanoporous catalytic solids. *Chem. Soc. Rev.* **39**, 4864. ([doi:10.1039/c0cs00100g](https://doi.org/10.1039/c0cs00100g))

79. Stallmach F, Gröger S, Künzel V, Kärger J, Yaghi OM, Hesse M, Müller U. 2006 NMR studies on the diffusion of hydrocarbons on the metal-organic framework material MOF-5. *Angew. Chemie Int. Ed.* **45**, 2123–2126. ([doi:10.1002/anie.200502553](https://doi.org/10.1002/anie.200502553))

80. Grissom TG, Sharp CH, Usov PM, Troya D, Morris AJ, Morris JR. 2018 Benzene, toluene, and xylene transport through UiO-66: diffusion rates, energetics, and the role of hydrogen bonding. *J. Phys. Chem. C* **122**, 16060–16069. ([doi:10.1021/acs.jpcc.8b03356](https://doi.org/10.1021/acs.jpcc.8b03356))

81. Zhou XL, Castro ME, White JM. 1990 Interactions of UV photons and low energy electrons with chemisorbed benzene on Ag(111). *Surf. Sci.* **238**, 215–225. ([doi:10.1016/0039-6028(90)90079-N](https://doi.org/10.1016/0039-6028(90)90079-N))

82. Torres-Knoop A, Balestra SRG, Krishna R, Calero S, Dubbeldam D. 2015 Entropic separations of mixtures of aromatics by selective face-to-face molecular stacking in one-dimensional channels of metal-organic frameworks and zeolites. *Chemphyschem.* **16**, 532–535. (doi:10.1002/cphc.201402819)

83. Renouprez AJ, Fouilloux P, Candy JP, Tomkinson J. 1979 Chemisorption of water on nickel surfaces. *Surf. Sci.* **83**, 285–295. (doi:10.1016/0039-6028(79)90493-X)

84. Passos AR, Rochet A, Manente LM, Suzana AF, Harder R, Cha W, Meneau F. 2020 Three-dimensional strain dynamics govern the hysteresis in heterogeneous catalysis. *Nat. Commun.* **11**, 1–8. (doi:10.1038/s41467-020-18622-2)

85. Cho KH, Mileo PGM, Lee JS, Lee UH, Park J, Cho SJ, Chitale SK, Maurin G, Chang JS. 2021 Defective Zr-fumarate MOFs enable high-efficiency adsorption heat allocations. *ACS Appl. Mater. Interfaces* **13**, 1723–1734. (doi:10.1021/acsami.0c15901)

86. Ortiz-Roldan JM, Balestra SRG, Bueno-Perez R, Calero S, Garcia-Perez E, Catlow CRA, Ruiz-Salvador AR, Hamad S. 2022 Data from: understanding the stability and structural properties of ordered nanoporous metals towards their rational synthesis. Figshare. (doi:10.6084/m9.figshare.c.6198515)

21

royalsocietypublishing.org/journal/rspa   *Proc. R. Soc. A* **478**: 20220201